JOURNAL OF CATALYSIS **167,** 106–117 (1997)
ARTICLE NO. CA971537

In Situ Study of Redox and of p-Type Semiconducting Properties of Vanadyl Pyrophosphate and of V–P–O Catalysts during the Partial Oxidation of *n*-Butane to Maleic Anhydride

Jean-Marie Herrmann,*,[1] Philippe Vernoux,*,† Kossi E. Béré,† and Michel Abon†

*URA au CNRS, "Photocatalyse, Catalyse et Environnement," Ecole Centrale de Lyon, B.P. 163, 69131 Ecully Cédex, France; and †Institut de Recherches sur la Catalyse, CNRS, 2 avenue Albert Einstein, 69626 Villeurbanne Cédex, France

Received April 15, 1996; revised September 20, 1996; accepted November 14, 1996

In situ **electrical conductivity measurements have been performed on vanadyl pyrophosphate samples as a function of their preparation temperature and on V–P–O catalysts as a function of their activation time. In agreement with X-ray diffraction results, electrical conductivity has shown that heat treatment of vanadyl pyrophosphates between 450 and 800°C results in a less conducting state corresponding to a very crystalline form. Such a stabilized form can already be reached at a temperature between 600 and 700°C. For V–P–O catalysts, electrical conductivity decreased as a function of the activation time, t_{act}, under the reaction mixture, reaching a steady value for $t_{act} \geq 84$ h. Both types of solids were found to be p-type semiconductors with positive holes as the main charge carriers. During subsequent exposures to *n*-butane and to oxygen at reaction temperature (400°C), it was confirmed that vanadyl pyrophosphate constitutes the main phase of efficient V–P–O catalysts working with some excess of surface oxygen probably in relation with the presence of V^{5+} species. The recorded changes in conductivity upon exposure to reactants provide illustrative evidence of a redox (Mars and van Krevelen) mechanism. The long activation period necessary to produce a high yield of maleic anhydride corresponds to structural and chemical changes of the surface which accommodates the reaction mixture and gives rise to active and selective sites able to convert *n*-butane to maleic anhydride.** © 1997 Academic Press

INTRODUCTION

Vanadium–phosphorus–oxygen compounds (V–P–O) constitute the principal phases able to catalyze the direct mild oxidation of *n*-butane to maleic anhydride. A special issue of *Catalysis Today* has recently been devoted to this topic (1). Although the main phase of V–P–O catalysts is constituted by vanadyl pyrophosphate ($(VO)_2P_2O_7$), the composition of real V–P–O catalysts is actually complex since they contain substantial amounts of V^{5+} ions (2–4). Numerous questions relating to the active phase on the surface of the working catalyst are still unclear. As stated recently by Centi in a critical review (5), the nature, amount, distribution, and evolution of V^{5+} phosphate phases during catalytic tests require further investigations.

Most efficient VPO catalysts for maleic anhydride formation are generally prepared by a long-term activation (e.g., 3000 h) of the precursor, $VO(HPO_4)$, 0.5 H_2O under reaction conditions, i.e., under *n*-butane/air flow at a temperature in the 380–450°C range. Recent work by Volta *et al.* (6–8), using Raman spectroscopy and other techniques, and by Overbeek *et al.* (9), using DRIFTS and XRD, has pointed out the importance of studying the changes in the catalyst in the course of the activation process. In a more recent study by two of us (10), V–P–O catalysts have been characterized as a function of the activation time at 400°C under the reaction mixture by using several techniques: XRD, ^{31}P-NMR (magic angle spinning and spin-echo mapping), and XPS. It was found that during activation, the V–P–O catalysts undergo progressive reduction, the δ-$VOPO_4$ phase, responsible for most of the V^{5+} ions present, being reduced to $(VO)_2P_2O_7$. It was clearly observed that the selectivity to maleic anhydride increased progressively as the ratio V^{4+}/V^{5+} increased under the reaction mixture. It is usually considered that the best catalyst requires an optimal value of this ratio.

Very few studies have been concerned with the electrical properties of vanadium phosphate phases. It has been shown that three of the V^{5+}-based vanadyl phosphate ($VOPO_4$) phase (α, β, and γ) are extrinsic n-type semiconductors, whereas δ-$VOPO_4$ is a p-type semiconductor (11). However, this phase is easily reduced, at least in the surface region, into $(VO)_2P_2O_7$ under butane. For the former three phases, it could be easily explained that $VOPO_4$ operates via a redox process, butane being oxidized to butene by consumption of surface anions and creation of anion vacancies, which were subsequently filled by dissociated oxygen coming from the gas phase.

In the present work, V^{4+}-containing phases have been characterized by electrical conductivity measurements with respect to (i) the influence of the preparation temperature of vanadyl pyrophosphate; (ii) the influence of the

[1] To whom correspondence should be addressed.

0021-9517/97 $25.00

activation time of V–P–O catalysts; (iii) the influence of pure gas atmospheres (oxygen or *n*-butane); and (iv) the influence of the reaction mixture. A comparison between the two types of solids has also been established, since it is known from the above-mentioned references that real V–P–O catalysts are mainly constituted by pyrophosphate.

EXPERIMENTAL

1. Preparation of Solids

The common precursor was prepared in an organic medium (12) using *i*-butanol. V_2O_5 (11.8 g) was added to H_3PO_4 (85%), with a $P/V = 1.1$ atomic ratio. After refluxing (16 h) under a nitrogen flow, a light blue-green suspension was obtained and then separated by filtration. The resulting precipitate was washed (with *i*-butanol and ethanol) and dried (16 h, 100°C). The XRD pattern of the precursor showed that a well-crystallized $VO(HPO_4)$, 0.5 H_2O phase was obtained.

1.1. Preparation of $(VO)_2P_2O_7$ samples. Five $(VO)_2P_2O_7$ samples have been prepared by calcination under a dried nitrogen flow of the precursor $VO(HPO_4)$, 0.5 H_2O at 450, 500, 600, 750, and 880°C for at least 40 h. For each preparation the temperature was first linearly raised (1°C/min) up to the steady temperature of preparation (t_{prep}). These catalysts were denoted Pyro-450, Pyro-500, Pyro-600, Pyro-750, and Pyro-880, respectively. Indeed, this series of catalysts is not representative of the usual industrial catalysts. The aim was to produce single-phase $(VO)_2P_2O_7$ to study the effect of the temperature of preparation and therefore mainly the crystallization state.

The X-ray diffraction patterns of representative samples, shown in Fig. 1, are typical of the $(VO)_2P_2O_7$ phase. Note, however, that the X-ray reflections become less and less intense and broader when the temperature of preparation decreases from 880 to 450°C. This change is most likely to be the result of an increasing structural disorder (13), especially in the stacking arrangement of basal (200) planes (23°, 2θ) with also a decrease in the size of the crystalline domains at lower temperatures.

1.2. Preparation of V–P–O samples. Starting with the same precursor in a microreactor, four separate preparations have been made under the same flow of the reaction mixture, (n-$C_4H_{10}/O_2/He = 1.6/18/80.4$) at atmospheric pressure. Note that the composition of the gas mixture was similar to the usual *n*-butane/air mixture used to activate industrial VPO catalysts. The total gas flow was 2.4 liter h^{-1} with a VSHV = 1500 h^{-1}. The temperature was linearly increased (0.5°C min^{-1}) from room temperature up to 400°C. This initial treatment was identical for the four experiments. The only difference was the time on stream at 400°C:

0.1 h (VPO-0.1),
8 h (VPO-8),
84 h (VPO-84),
132 h (VPO-132).

The catalysts were quenched after these different activation times by switching off the oven. The by-passed glass reactor was cooled down rapidly to room temperature. The catalysts were then rapidly put into small glass flasks which were filled with argon and closed. Their X-ray diffraction patterns are given in Fig. 2 mainly indicate the presence of a poorly crystallized $(VO)_2P_2O_7$ phase. Indeed, an equilibrated industrial V–P–O catalyst displays stable and optimal catalytic performance only after at least 2000 or 3000 h

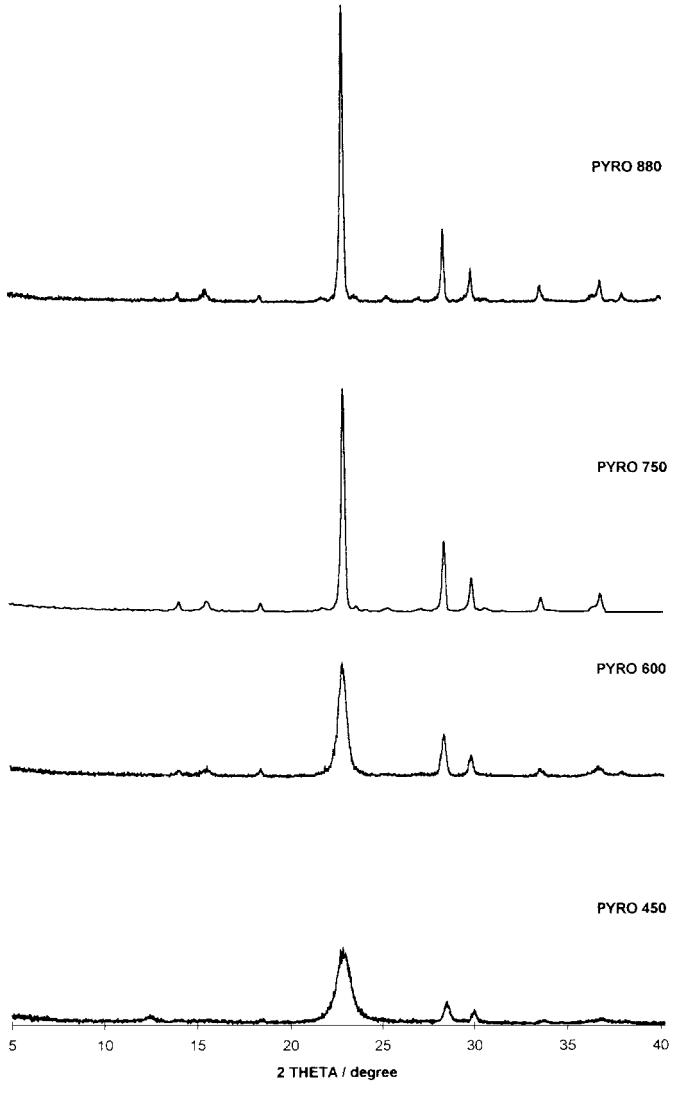

FIG. 1. X-ray diffraction patterns of vanadium pyrophosphate ($(VO)_2P_2O_7$) sample.

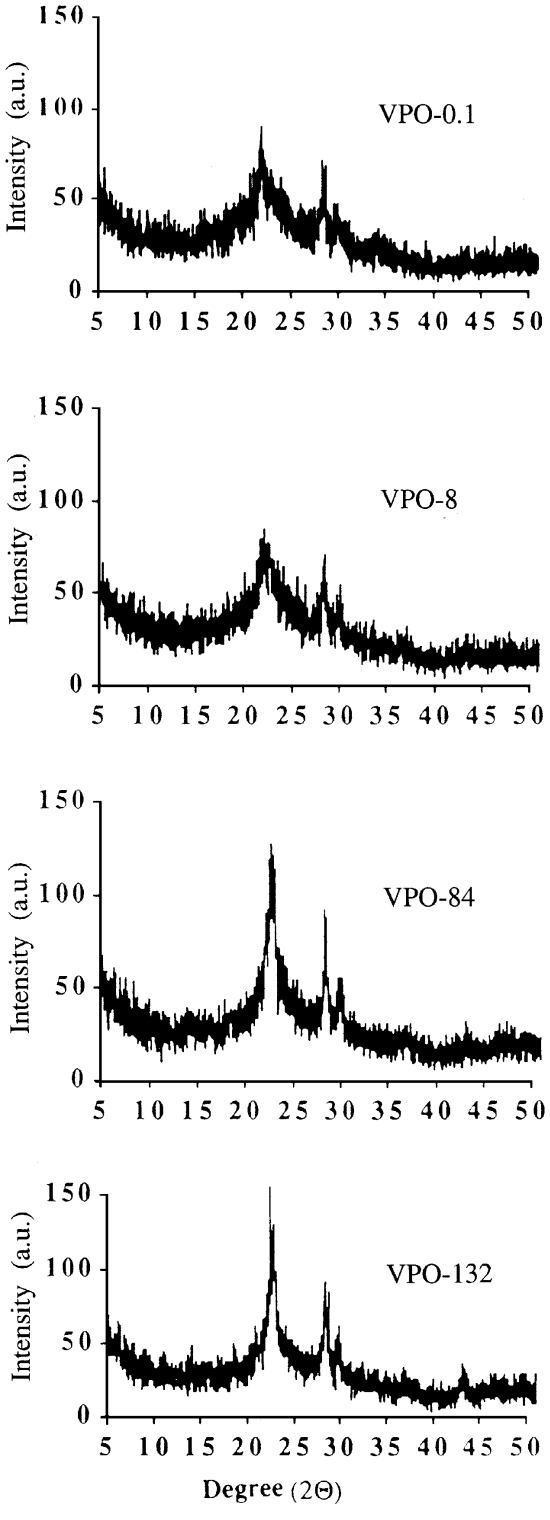

FIG. 2. X-ray diffraction patterns of V–P–O catalysts.

on stream. On the laboratory scale it is not possible to reproduce such a long activation time. However, after 132 h the catalytic performances are already fairly good and not very different from a truly stabilized solid.

2. Electrical Conductivity Cell

The electrical conductivity of the different samples has been investigated by using a cell specially designed to study the electronic interactions between powdered samples and various gaseous atmospheres (14). This cell has previously been employed for studying pure, doped, mixed oxides, sulfides, and metal/semiconductor catalysts.

About 120 mg of catalyst was placed between two platinum electrodes between which they were compressed under a constant mechanical pressure of ca. 10^5 Pa which is compatible with good interparticle electrical contacts and with a good gas–solid interaction over the whole surface of the solid. The temperature of each electrode was given by a thermocouple whose wires also used as connections for electrical measurements. The electrical resistance of the samples was measured with various *R*-meters according to the range investigated: a Kontron multimeter (model DMM 4021) for resistances lower than 2×10^6 ohm (D.C. voltage, 1 V) or with a digital teraohmmeter (Guildline Instruments, Model 9520) for higher values (D.C. voltage from 1 to 10 V). It has been previously shown that powdered semiconducting oxides behave as massive conductors (14) and the electrical conductivity (σ) of the powdered samples can be formally written as

$$\sigma = 1/\rho = 1/R \times t/S, \qquad [1]$$

where ρ is the resistivity, R is the electrical resistance, and (t/S) is the geometric factor (t is thickness (generally chosen between 0.4 and 0.5 cm) and S is the section area of the electrodes (diameter 1.00 cm)). Conductivity measurements carried out on powders provide intrinsic bulk values for the material, when surface and bulk conductivities are similar. In that case, the experiments are identical to those carried out on single crystals, for which

$$\sigma = nq\mu \qquad [2]$$

where n and μ are, respectively, the concentration and the mobility of the main charge carriers and q is the elementary charge of the electron. For a powdered sample, the conductivity σ can be written as

$$\sigma = An, \qquad [3]$$

where A is a coefficient of proportionality which remains constant during the experiment and includes, besides q and μ, textural parameters, such as the number of interparticle contact points. Since, in this work, all the samples have BET surface areas of the same order of magnitude, coefficient A can be considered as nearly constant whatever the solid. Hence, semiquantitative comparisons between solids may be made and electrical conductivity measurements provide an estimate of the variations in the concentration of the

TABLE 1

Catalytic Performances of Vanadium Pyrophosphate Catalysts

Catalyst	A ($m^2 \cdot g^{-1}$)	C (%)	S_{MA} (%)	S_{CO_x} (%)	V_s ($mol \cdot s^{-1} \cdot g^{-1} \times 10^8$)	V_i ($mol \cdot s^{-1} \cdot m^{-2} \times 10^8$)
Pyro-450	14.5	19	80	19	18.9	1.3
Pyro-600	12.8	18	61	38	17.7	1.9
Pyro-750	4.5	17	59	40	21.2	4.7
Pyro-880	4.0	15	42	39	11.7	2.9

main charge carriers as a function of physical parameters such as temperature, oxygen pressure, nature, and pressure of other gases, under conditions as close as possible to those of the catalytic reaction. Upon exposure to a gas atmosphere, it is likely that conduction effects at the surface dominates as seems to be the case for the present results and was considered to be true for other oxide catalysts (15–17). It is important to stress that values of σ are relative and not absolute.

3. Catalytic Tests

Catalytic tests have been performed in a flow microreactor in the temperature range 380–440°C. The composition of the gas mixture was n-C_4H_{10}/O_2/He 1.6/18/80.4 at atmospheric pressure. The total gas flow was in the range 1.8–2.4 l h^{-1} with a VSHV equal to 1500 h^{-1}. On-line analysis of reactants and products was achieved by gas chromatography using three different columns to separate hydrocarbons, oxygenates, and CO_x. Sampling valves and tubing were located in a hot box (140°C). The carbon mass balance was better than 97–98%.

RESULTS AND DISCUSSION

1. Catalytic Performances of Pyrophosphate and V–P–O Samples

The present work is mainly devoted to the electrical conductivity properties of these solids. However, it is indeed first important to give a general survey of their catalytic performances in the n-butane reaction at 400°C.

1.1. Pyrophosphate catalysts. Table 1 summarizes the results for $(VO)_2P_2O_7$ samples prepared at different temperatures. Besides the BET surface area (A), Table 1 compares the n-butane conversion (C), the selectivity for MA (S_{MA}) and for CO_x (S_{CO_x}), the specific activity (V_s) and the intrinsic activity (V_i) for the conversion of butane. The activity of the four studied catalysts is not much different; the most active appears to be the sample prepared at 750°C. The main difference concerns the selectivity for MA: the lower the temperature of preparation, the higher S_{MA}.

1.2. V–P–O catalysts. Table 2 shows the evolution of the catalytic properties of a V–P–O catalyst with the time of activation under the reaction mixture at 400°C. The results have been obtained on the basis of four seperate experiments. More details can be found in a previous paper (10). It is clear that catalytic performances are improving with time on stream in relation with the development of the $(VO)_2P_2O_7$ active phase as previously described (10). The catalytic properties are first improving at a high rate at the beginning of the activation but the changes become slower with time on stream and after about 84 h we observed a definite trend for a stabilization. However, as already stated in subsection 1.2 truly stable catalytic performance would require a much longer time, 2000 or 3000 h.

2. Electrical Conductivity Study of the Influence of the Temperature of the Preparation of the Vanadyl Pyrophosphate

As mentioned in the Introduction, the industrial catalysts which are active and selective in the mild oxidation of n-butane to maleic anhydride are obtained by a long activation period under the reaction mixture at 400°C. They are mostly constituted of vanadyl pyrophosphate. Their catalytic properties strongly depend on their structural and textural properties which originate from their initial temperature of preparation for a given hemihydrate precursor. This is the reason why several solids have been synthesized at different temperatures between 450 and 800°C.

Since the pyrophosphate samples are constituted of a V^{4+} phase, electrical conductivity measurements were

TABLE 2

Physical Characteristics and Catalytic Performances of V–P–O Catalysts

Catalyst	A ($m^2 \cdot g^{-1}$)	V^{4+}/V^{5+} (XPS)[a]	C (%)	S_{MA} (%)	S_{CO_x} (%)	V_s ($mol \cdot s^{-1} \cdot g^{-1} \times 10^{+8}$)	V_i ($mol \cdot s^{-1} \cdot m^{-2} \times 10^{+8}$)
VPO-0.1	10.5	1.1	22	34	64	13.3	1.3
VPO-8	7.6	1.3	26	48	51	15.7	2.0
VPO-84	14.8	1.5	55	66	32	33.2	2.2
VPO-132	19.4	1.7	65	69	30	39.1	2.1

[a] Value taken from Ref. (10).

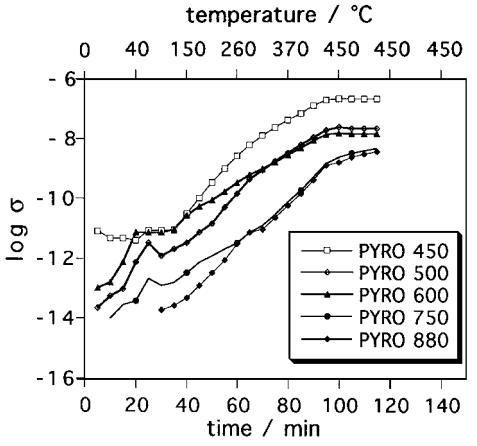

FIG. 3. $\log\sigma = f(t)$ during temperature-programmed heating of vanadium pyrophosphate samples under dynamic vacuum from room temperature to 450°C (heating rate: 5°C/min). σ in ohm^{-1} cm^{-1}.

performed in vacuum which was chosen as an inert reference atmosphere able to conserve the valence +4 for vanadium ions. The solids were promptly outgassed at room temperature under dynamic primary vacuum and then heated to 450°C, at a heating rate of 5°C/min.

The kinetic variations $\log\sigma = f(t)$ during temperature-programmed heating are given in Fig. 3. The different curves are regularly ascending with, however, a small peak at ca 100°C. This has been attributed to surface dehydration with the suppression of surface conduction by protons which can hop from one adsorbed water molecule to another one (18). The presentation of the curves of Fig. 3 within the frame of a $\log\sigma$ vs. $1/T$ plot is given in Fig. 4. A linear variation of $\log\sigma = f(1/T)$ is only observed at higher temperatures. This means that in this temperature region all the solids behave as semiconductors whose electrical conductivities vary exponentially with temperature according

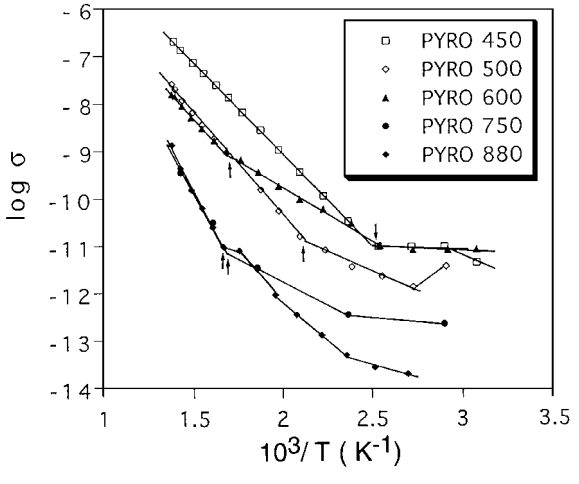

FIG. 4. Plots of $\log\sigma = f(1/T)$ of curves of Fig. 3.

TABLE 3

Physical and Electrical Characteristics of Vanadium Pyrophosphate Samples

Samples	BET surface area (m^2/g)	E_c (kJ/mol)	Threshold temperatures (t_{th})(°C)
Pyro-450	14.5	73.2	121
Pyro-500	22	84.5	202
Pyro-600	9.3	80.6	345
Pyro-750	4.5	134.8	348
Pyro-880	4	138.1	324

to the familiar law

$$\sigma = \sigma_0 \exp(-E_c/RT), \qquad [4]$$

where σ_0 is the preexponential factor and E_c is presently the "dynamic" activation energy of conduction (dynamic, because σ is measured during the temperature program and not at steady state at constant T). The linear parts of the plots commence at temperatures denoted "threshold temperatures"(t_{th}), which are indicated by vertical arrows in Fig. 4 and are also given in Table 3. This table also contains the calculated activation energies of conduction (E_c) and the BET surface areas.

At the end of the temperature ramp, the electrical conductivities were measured as a function of time until the establishment of the steady state. These final values obtained at the equilibrium σ_{eq} are plotted as a function of the preparation temperature (t_{prep}) under nitrogen flow (Fig. 5A). These values were obtained after a duration which increases with t_{prep}. Figure 5 also shows for comparison the changes with t_{prep} of the threshold temperature (t_{th}) and the activation energy of conduction E_c.

2.1. Interpretation of the conductivity variations. It can be observed that all the different parameters of the electrical conductivity of the different "Pyro"samples change with the preparation temperature (t_{prep}) used for their preparation under a nitrogen flow.

The higher t_{prep}, the lower the electrical conductivity either during the heating process under vacuum (Figs. 3 and 4) or at steady state at 450°C (Fig. 5). The higher t_{prep}, the higher the activation energy of conduction and the higher the threshold temperature (t_{th}) above which appears a regular semiconductivity (Fig. 5). All these variations indicate a stabilization in the variations of the different electrical parameters for preparations temperatures (t_{prep}) comprised between 600 and 700°C.

In agreement with the XRD patterns (Fig. 1), it can be inferred that when t_{prep} is increased, the $(VO)_2P_2O_7$ samples gradually acquire a better state of crystallization with an increase of the particle size as evidenced by the decrease of the BET surface area (Table 1). In addition, structural

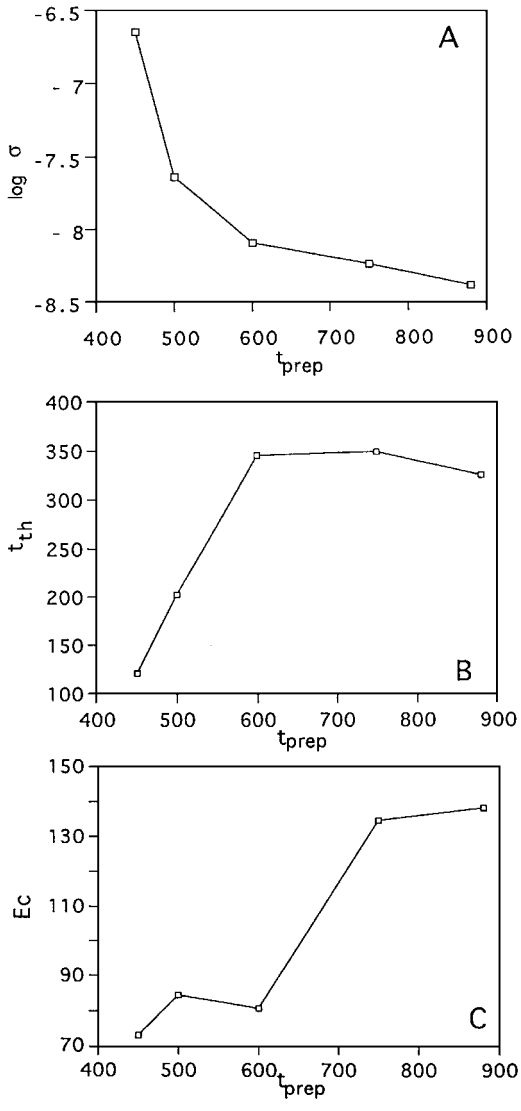

FIG. 5. Variations as a function of the preparation temperature (t_{prep}) (in °C) (i) of the electrical conductivity at steady state (curve A); (ii) of the threshold temperature (t_{th}) (see definition in the text) (curve B): and (iii) of the dynamic activation energy of conduction E_c (in kJ/mol) (curve C).

defects which can act as sources of charge carriers in the case of extrinsic semiconductors are gradually erased. It can actually be seen that steady-state conductivities follow the same variations as a function of t_{prep} as the specific surface areas (Table 1). The samples treated at high t_{prep} tend to become intrinsic semiconductors with low conductivities and large activation energies of conduction and with a decreasing part of surface conductivity linked to surface defects and to interaction with the gas phase.

2.2. Consequences for catalysis. The Pyro samples have been tested in the *n*-butane oxidation reaction (see Table 1). The optimum intrinsic rate for butane conversion (in mol s^{-1} m^{-2}) was found for Pyro-750. However, the highest selectivity to maleic anhydride has been measured for Pyro-450, i.e., for the solid which has the highest electrical conductivity and presumably the highest structural disorder.

The formation of maleic anhydride requires oxidizing sites for oxygen insertion in the steps following the initial oxidative dehydrogenation leading to the butadiene intermediate. It is usually believed that such oxidizing sites are associated with the presence of a suitable amount of V^{5+} species, maybe V^{5+}=O vanadyls.

Reversible surface oxidation of some V^{4+} surface ions probably occurs more easily on a surface not too perfectly crystallized insofar as surface defect and structural disorder must improve the reactivity and facilitate a suitable oxidation rate.

3. Electrical Conductivity Study of the Influence of the Activation Time of V–P–O Catalysts under Reaction Mixture

We have previously shown (10) that the changes of the catalytic performances with the time of activation on stream can be correlated with a progressive reduction of V^{5+} phases into $(VO)_2P_2O_7$. We have observed an increase with time of the V^{4+}/V^{5+} ratio both in the bulk (^{31}P-NMR) and on the surface (XPS). The (V^{4+}/V^{5+}) ratio determined by XPS is reported in Table 2.

As for Pyro catalysts V–P–O catalysts were studied under dynamic primary vacuum to conserve the main V^{4+} ionic state of vanadium. Electrical conductivity was measured on VPO samples previously activated at different activation times (t_{act}) as a function of time and temperature, from room temperature to 300°C (heating rate, 5°C/min.). The kinetic curves of $\log\sigma = f(t)$ are presented in Fig. 6 and the corresponding reciprocal temperature transforms ($\log\sigma = f(1/T)$ are presented in Fig. 7.

The σ values obtained at steady state (300°C) are given in Fig. 8. It appears that steady-state values of σ become

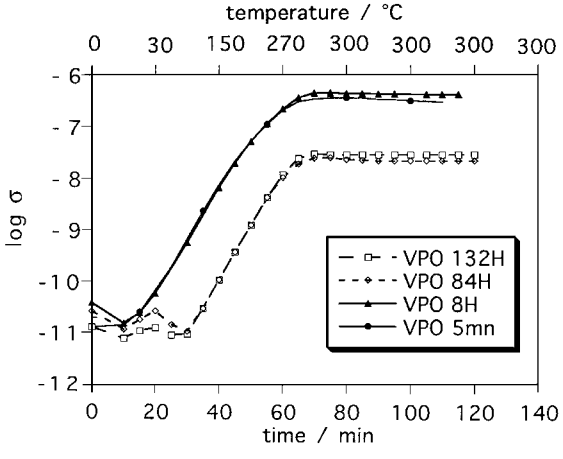

FIG. 6. $\log\sigma = f(t)$ during temperature-programmed heating of V–P–O samples under dynamic vacuum from room temperature to 300°C (heating rate, 5°C/min).

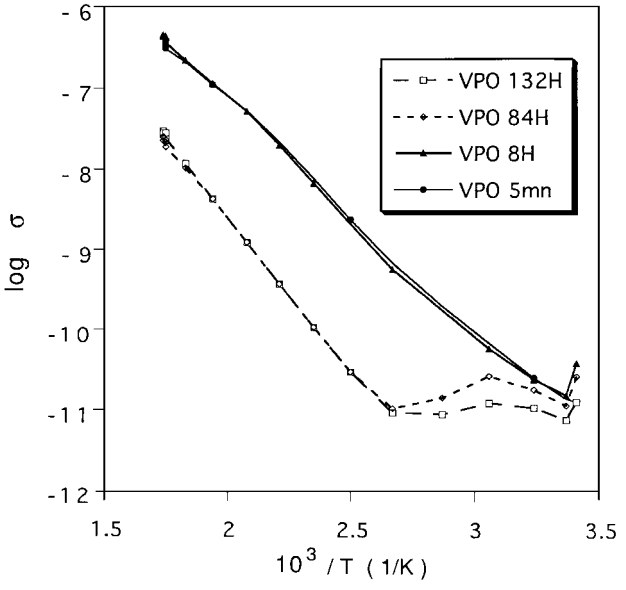

FIG. 7. Plots of $\log\sigma = f(1/T)$ of curves of Fig. 6.

progressively independent of the activation time (t_{act}) for $t_{act} \geq 84$ h. For the Pyro samples we observed a correlation (Fig. 5) between the steady-state electrical conductivity under vacuum and the crystallization state: the lower the temperature of preparation (t_{prep}), the higher the conductivity. For the V–P–O catalyst activated at 400°C, the electrical conductivity is comparable to the value recorded for Pyro-450, at least for short activation times (VPO-0.1 and VPO-8) as shown in Fig. 8. With time of activation the crystallization somewhat improves as evidenced by XRD (Fig. 2) and as for the Pyro samples, the conductivity decreases (Fig. 8) and becomes close to the value measured for Pyro-500 (Fig. 5A). The steady-state σ values could also depend on other factors

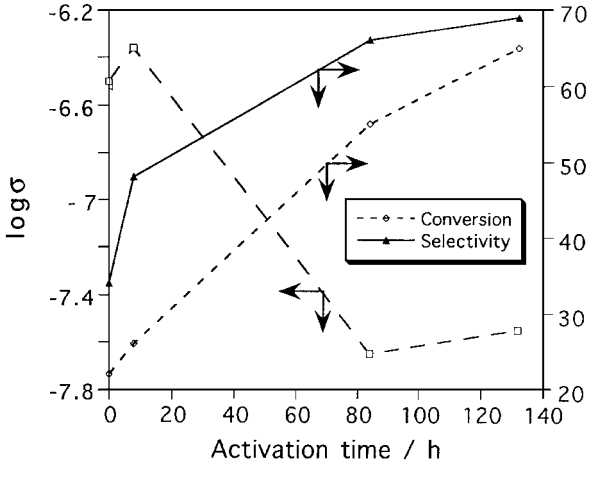

FIG. 8. V–P–O catalysts: variations as a function of the activation time under reaction mixture of the electrical conductivity at steady state (in $ohm^{-1}\,cm^{-1}$) of the conversion of *n*-butane (in %) and of the selectivity to maleic anhydride (in %).

such as the surface area (Tables 1 and 2) and especially for the VPO series the changes in the relative amount of V^{5+} and V^{4+} phases (10) indicated by the V^{4+}/V^{5+} ratio given in Table 2.

Maleic anhydride is the main reaction product. It is therefore not surprising that the catalytic performance (conversion and selectivity) increases with the activation time in a similar way (Fig. 8). After ca. 84 h, the steady state is not achieved but the major part of the catalytic changes have already been obtained. The electrical conductivity roughly varies conversely with the catalytic performance and is already stabilized for $t_{act} \geq 84$ h.

A better knowledge of the surface reactivity of both Pyro and V–P–O catalysts can be obtained from electrical conductivity measurements performed under each of the two reactants as well as under the reaction mixture. This is the object of the next Section.

4. *Influence of n-Butane and of Oxygen on the Electrical Conductivity of $(VO)_2P_2O_7$ and V–P–O Catalysts*

To obtain information on the solids under conditions as close as possible to those of catalysis, the electrical conductivity measurements were performed at reaction temperature (400°C) during sequential periods under butane and under oxygen at partial pressures identical to those of the reaction mixture (butane pressure, 11 Torr; oxygen pressure, 125 Torr) (1 Torr = 133.3 Pa).

4.1. $(VO)_2P_2O_7$ pyrophosphate catalysts. After heating the solids under vacuum from room temperature to 400°C at a heating rate of 5°C/min, *n*-butane was introduced in contact with the solid. Immediately, the electrical conductivity decreased abruptly from 1 to 3 orders of magnitude (Figs. 9A and 10). Despite the poor reactivity of alkanes, butane must be considered as a reductant and, consequently, the behavior of pyrophosphate samples is typically that of a p-type semiconductor. For Pyro-450 as well as for the VPO-400 sample (activated for 132 h), the electrical conductivity decreases regularly and tends to a plateau within half an hour (Fig. 9A). By contrast, for Pyro-600 and Pyro-750, the electrical conductivity first strongly decreases initially and then increases slowly to reach the plateau corresponding to steady state under 11 Torr of *n*-butane. This phenomenon is reproducible and can be repeated in a second sequence under butane. It is more pronounced when the temperature of preparation increases (compare Figs. 10A and 10B). The kinetic curves $\sigma = f(t)$ in butane correspond to the combination of two opposite phenomena, a strong initial reduction by butane followed by a kind of progressive reoxidation of the surface region.

After reaching the steady state under butane, the gas phase was promptly evacuated and replaced by pure oxygen under 125 Torr. For all samples, the electrical conductivity increased immediately and tended to a plateau (Figs. 9 and 10). This behavior confirms the p-type character of

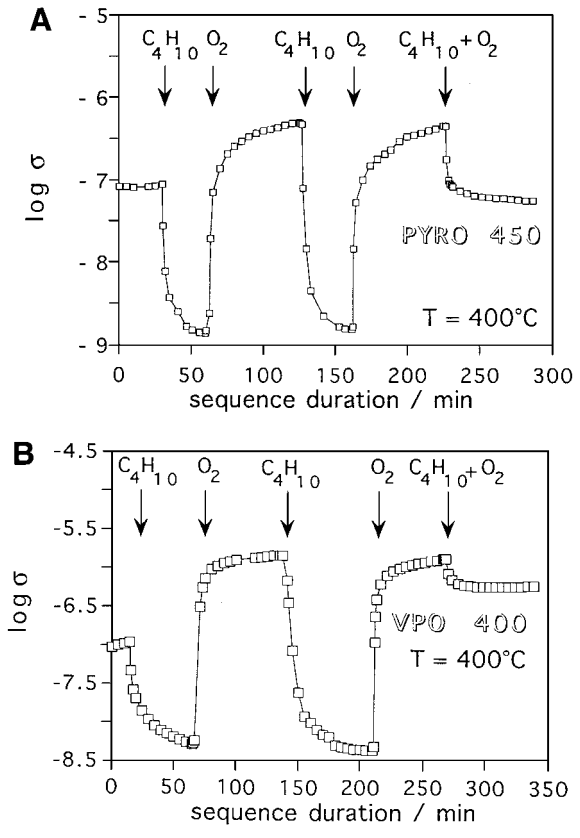

FIG. 9. Variations of the electrical conductivity at 400°C under sequential exposures to butane (11 Torr) and to oxygen (125 Torr) and under reaction mixture for Pyro-450 and VPO-400 samples.

$(VO)_2P_2O_7$, since for oxide semiconductors, the p-type criterion is $d\sigma/dP_{(O_2)} > 0$.

The p-type character is a fundamental feature for pyrophosphate or VPO samples, since it is observed both under reducing or under oxidizing conditions (Figs. 9 and 10). In addition, it is reproducible and typical of a redox mechanism since the repetition of the same n-C_4H_{10}/O_2 sequences provides identical variations of σ (Figs. 9 and 10). It can be recalled that all bulk $VOPO_4$ phases, except δ-$VOPO_4$, are, by contrast, of the n-type (11).

4.2. V–P–O catalysts. The same behavior was observed for V–P–O catalysts as exemplified by the V–P–O sample activated at 400°C for 132 h (Fig. 9B). Repeated sequences in n-C_4H_{10} and in O_2 yielded reproducible variations. As Pyro samples, V–P–O catalysts are p-type semiconductors, whatever the conditions chosen. These similar electrical results confirm that V–P–O catalysts are mainly constituted of vanadyl pyrophosphate ($(VO)_2P_2O_7$) as previously stated from XRD patterns. The solids behave as redox relays according to the nature of the gas phase with which they have been placed in contact.

No direct and obvious quantitative relationships between $\Delta \log \sigma$ (for example when switching from butane to oxygen) and catalytic behavior could be established. This may be due to the complex influence of various parameters linked either to the solids (crystallite size and shape, mean oxidation state of vanadium, etc.) or to the difference in the type of apparatus (electrical conductivity measured in a static cell and catalytic data obtained in a flow reactor). Results in Figs. 9 and 10 must be considered as the qualitative responses of conductivity during exposures to each of the reactants, confirming that all the solids behave as p-type semiconductors.

5. *In Situ Electrical Conductivity Measurements on Pyrophosphate and V–P–O Catalysts during Reaction*

After the last sequence in oxygen at 400°C, O_2 was promptly evacuated and a reaction mixture containing 11 Torr n-C_4H_{10} and 125 Torr O_2 was introduced at the same temperature. This gas phase composition corresponds to that used in catalysis. Instantaneously, the electrical conductivity decreased and tended to a plateau located in between the high level under pure oxygen and the low level under pure n-butane (Figs. 9 and 10). When the reaction mixture was introduced after a last sequence in n-butane instead of oxygen (Fig. 10A), the electrical conductivity immediately increased. In all cases, the electrical behavior of

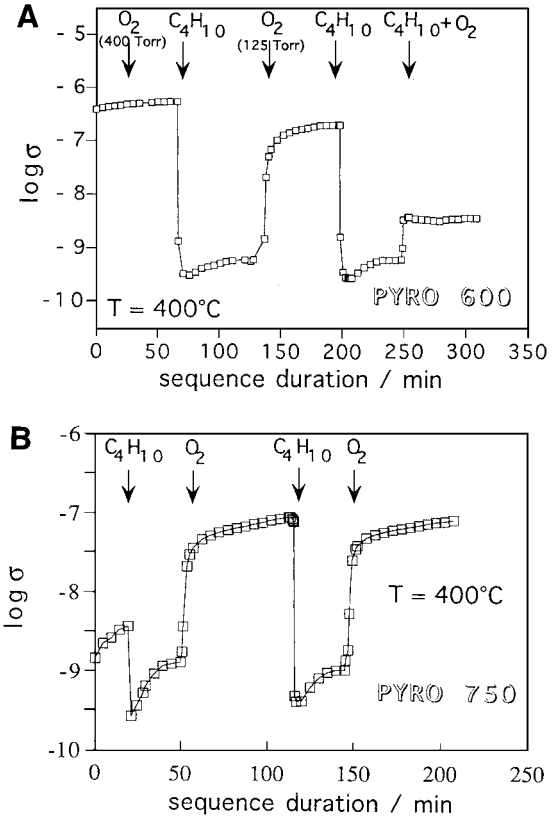

FIG. 10. As for Fig. 9 but for Pyro-600 and Pyro-750 samples.

Pyro samples confirmed the p-type character for the solids under catalytic reaction.

For V–P–O catalysts, the variations of σ were qualitatively the same, confirming vanadyl pyrophosphate ($(VO)_2P_2O_7$) as its main constituent. By comparing Figs. 9A and 9B relative to Pyro-450 and VPO-400, it appears that electrical conductivity values are very similar in all the sequences performed. It can be assumed from the preceding sections that they have fairly similar structural and textural properties, in agreement with XRD patterns and BET specific area measurements. Pyro samples and V–P–O catalysts display similar redox cycles. They play the role of redox relays able to be reduced by butane and reoxidized by oxygen in agreement with a Mars and van Krevelen mechanism. Indeed, both reactions occur simultaneously under the reaction mixture but actually they occur sequentially at the level of each active site according to the scheme

$$\text{oxidized cat.} + n\text{-}C_4H_{10} \rightarrow \text{reduced cat.} + \text{products}$$

$$\text{reduced cat.} + O_2 \rightarrow \text{oxidized cat.}$$

These redox cycles allow them to be selective in the very complex mild oxidation of *n*-butane to maleic anhydride, which involves 14 electrons, 4 oxydehydrogenation steps, one heterocyclization, and two insertions of O atoms into carbonyl groups per butane molecule transformed. The progressive adaptation of the catalyst to the reaction mixture to produce specific sites able to transform selectively C_4H_{10} to MA is illustrated by the long activation period under reaction mixture required by industrial V–P–O catalysts to become active and selective. The best illustration for these redox considerations, deduced from Figs. 9 and 10, is offered by the new design of the latest industrial reactors in which the circulating catalyst is considered as an oxidizing reactant which is reduced *in situ* under a butane stream and then reoxidized in an outer regenerator (19–21).

We have recently confirmed the redox mechanism of this reaction using $^{18}O_2$ in a recirculation reactor with on-line gas analysis by mass spectrometry (22). This study clearly showed that only lattice oxygen anions, belonging to a few surface layers, are involved in the formation of maleic anhydride and of CO_x.

6. *Correlation between p-Type Semiconductivity and Catalysis*

P-type conductivity is generally less often observed than n-type on oxide semiconductors (14). P-type conductivity can be encountered either on simple oxides such as NiO (23) or on binary oxides such as U–Sb–O oxides (24–26). Such a type of conductivity corresponds to an excess of oxygen in the solid.

In oxides such as NiO, p-type conductivity is due to the presence of cationic vacancies to which correspond electrical conductivity variations according to: $\sigma \propto P_{O_2}^{+1/n}$, n being a positive integer depending on the valency of the missing cation (14). Presently, σ was found to be independent of the oxygen pressure. Therefore, no vanadium V^{4+} nor $(VO)^{2+}$ cationic vacancies can be expected. P-type conductivity could be also accounted for by the existence of O_i interstitial species, as in U–Sb–O catalysts (23, 24). In that case, σ should depend on the oxygen partial pressure.

An alternative interpretation of the conductivity results could have been the effect of oxygen chimisorption on unsaturated V^{4+} surface ions. Since all the solids are p-type semiconductors, oxygen chimisorption would have produced an increase of σ with increasing P_{O_2}. Since σ is independent of P_{O_2} as mentioned above, the possible influence of the existence of oxygen ionosorbates such as O_2^- and O^- can be ruled out. However, we cannot discard the reversible oxidation of coordinatively unsaturated (CUS) V^{4+} ions which are known to exist at the surface of $(VO)_2P_2O_7$ as evidenced by its Lewis acidity (37–40). It has also been frequently claimed that the presence of a suitable amount of V^{5+} (either isolated ions or $VOPO_4$ patches) is essential for good catalytic performance (1, 3, 7). As recently discussed by Busca (41), the best formulation of the catalyst could be $V_2P_2O_{9+\delta}$, with some excess of surface oxygen due to the presence of pentavalent vanadium. Such an excess of oxygen with respect to the stoichiometry of $(VO)_2P_2O_7$ (V^{4+} phase) could explain the changes in electrical conductivity (induced by the reactants) which are typical of a p-type semiconductor.

Indeed, pentavalent vanadium would be present on the surface as isolated or nearly isolated V^{5+} species or patches of precursor of the δ-$VOPO_4$ phase. A thick surface layer of $VOPO_4$ can be discarded, especially α_{II}, γ, or β-$VOPO_4$ phases which behave as *n*-type semiconductors.

In the present case, p-type conductivity, with positive holes p^+ as the main charge carriers, must be correlated with the redox couple V^{4+}/V^{5+}. The simultaneous existence of both oxidation states for vanadium ions is a well known phenomenon, which has been detected by ^{31}P-NMR and by XPS (10). Using EXAFS and other techniques, Lopez Granados *et al.* (27) concluded to the presence of a significant amount of mixed-valence V^{IV}-V^{V} pairs within the pyrophosphate lattice. Therefore, a permanent electrochemical equilibrium can be assumed:

$$V^{5+} \leftrightarrow V^{4+} + p^+. \qquad [5]$$

Since vanadium ions are involved in vanadyl ions, Eq. [2] can also be written as

$$(V^{V}O)^{3+} \leftrightarrow (V^{IV}O)^{2+} + p^+. \qquad [6]$$

From the electrochemical point of view, a positive hole p^+ (or positon) corresponds to an electron vacancy in the valence band of O^{2-} anions. Such an electron vacancy (or

hole) can be filled by an electron hopping from a neighbor anion

$$O^{2-} + p^+ \leftrightarrow O^- . \qquad [7]$$

Holes are virtual positive charges ($q = e^+$) whose migration or transfer corresponds to that of electrons in the opposite direction. In Eq. [7], O^- anions correspond to the "chemical site" of a hole.

Butane activation requires the cleavage of a C–H bond from a methylene group as demonstrated by Pepera *et al.* (30). This initial cleavage is usually recognized as the rate determining step [1 and 3]. As discussed by Chaar *et al.* (31), such a dissociation is likely to be homolytic because it requires much less energy: about 400 $kJ \cdot mol^{-1}$ instead of about 1600 $kJ \cdot mol^{-1}$ for a heterolytic cleavage giving $R^- + H^+$ in the gas phase. As second hydrogen abstraction rapidly occurs leading to butene as the first reaction intermediate (1, 3, 30, 32, 33). In the present work, we indeed observed the formation of butenes as minor products in the catalytic test.

Since p-type conductivity is observed after the catalysts have been contacted with *n*-butane, it can be proposed that the initial activation step of the alkane is a C–H bond cleavage via the attack by a hole:

$$C_4H_{10} + p^+ \leftrightarrow C_4H_9^{\bullet} + H^+ . \qquad [8]$$

If one considers the equilibrium given in Eq. [7], Eq. [8] is equivalent to

$$C_4H_{10} + O^- \rightarrow C_4H_9^{\bullet} + O^{2-} + H^+ . \qquad [8']$$

It is interesting to notice that the addition of Eqs. [5] and [7] gives

$$V^{5+} + O^{2-} \leftrightarrow V^{4+} + O^- . \qquad [9]$$

Equation [9] represents a charge transfer reaction which could occur especially at defect sites, as already proposed by Chaar *et al.* (31), Matsuura (34), and Szakacs *et al.* (35). Such a reaction provides a very reactive oxygen species, O^-, which could be responsible for butane activation according to Eq. [8′]. Since the works of Aika and Lunsford (36), it has been known that alkane oxydehydrogenation may occur with the intermediate of O^- species on oxide catalysts.

The next step leading to the transient formation of the olefin could also involve p^+ holes, equivalent to O^-:

$$C_4H_9^{\bullet} + p^+ \rightarrow C_4H_8 + H^+ \qquad [10]$$

$$C_4H_9^{\bullet} + O^- \rightarrow C_4H_8 + O^{2-} + H^+ . \qquad [10']$$

Water elimination then probably proceeds via the intermediate formation of hydroxyl groups:

$$2\,O^{2-} + 2\,H^+ \rightarrow 2\,OH^- \qquad [11]$$

$$2\,OH^- \rightarrow H_2O + O^{2-} . \qquad [12]$$

Equations [8] and [10] correspond to the consumption of the main charge carriers (p^+) as illustrated by the decrease of conductivity upon butane exposure (Figs. 9 and 10). The initial oxydehydrogenation of butane to butenes consumes a surface anion of the solid. This oxygen vacancy must be healed by gaseous oxygen in order to reoxidize the solid:

$$1/2\,O_2(g) \rightarrow O^{2-} + 2\,p^+ . \qquad [13]$$

As the reoxidation creates p^+ charges, Eq. [13] accounts for the steep increase of the electrical conductivity as soon as the reduced catalyst is exposed to gaseous oxygen (Figs. 9 and 10).

Indeed, the mass balance of Eqs. [8–13] corresponds to

$$C_4H_{10} + 1/2\,O_2 \rightarrow C_4H_8 + H_2O . \qquad [14]$$

The prevalent role of positive holes (p^+) in the proposed mechanism stems from the fact that they are known as strong oxidizing agents. In heterogeneous photocatalysis, such holes oxidize alkanes into corresponding aldehydes and ketones around room temperature (28, 29).

In a previous work (37), we have shown that V–P–O catalysts and especially $(VO)_2P_2O_7$ display acidic properties with a significant number of Lewis sites of medium strength. Such Lewis sites can be associated with coordinatively unsaturated (CUS) V^{4+} ions (38–40). Recently, Gai and Kourtakis (42) confirmed the presence of anion vacancies associated with Lewis acidic centers on butane-reduced $(VO)_2P_2O_7$ catalysts, using high–resolution electron microscopy. The catalytic partial oxidation of butane into maleic anhydride has been correlated with surface Lewis acidity on $(VO)_2P_2O_7$ (37, 40, 43, 44). In order to account for the role of surface acidity on pyrophosphate catalysts, it may be proposed that the site responsible for the initial butane activation would be an ion pair constituted of a CUS V^{4+} and a O^- species. Such a couple is expected to polarize the butane molecule and would then facilitate the C–H bond cleavage. The role of the reactive O^- species consists in the abstraction of a hydrogen atom as proposed in Eq. [8′]. A second hydrogen atom could be simultaneously abstracted by a V^{4+} ion, according to a concerted mechanism already discussed by Busca *et al.* (39). Alternatively, the secondary butyl radical (CH_3–$^{\cdot}CH$–CH_2–CH_3) formed according to Eq. [8′] could also coordinate with V^{4+} (leading to V^{3+}–C_4H_9). Such a bonding would be promoted by the negative polarization of the butyl radical.

It is well known that in a long-term activated catalyst (3000 h) the mean oxidation state of vanadium is only very slightly higher than 4 (3) with therefore only a few surface V^{5+} species, probably in mixed valence pairs V^{IV}-V^{V} as suggested by López-Granados *et al.* (27). Although the accurate value of the optimal V^{4+}/V^{5+} surface ratio is still not definitively established, we feel that it could be comprised

between 5 and 8 (45). The steady-state surface concentration of V^{4+}–O^- coming from the charge transfer reaction (Eq. [9]) would therefore be fairly low. This statement appears to be consistent with the low apparent energy of activation for a reaction performed at about 400°C: we measured about 70 $kJ \cdot mol^{-1}$ for the pyrophosphate samples studied in the present work. This fairly low activation energy suggests that the sites responsible for butane activation are scarce but quite active. If O^- species were too numerous on the surface, they might well promote butane combustion instead of partial oxidation.

CONCLUSIONS

The present electrical conductivity measurements have established the p-type character of $(VO)_2P_2O_7$ which is considered as the active phase in the selective partial oxidation of butane. *In situ* changes of the electrical conductivity in the presence of reactants or under reaction mixture provide a clear and direct evidence for a redox mechanism with consumption of surface lattice oxygen. Such a redox mechanism requires the presence of V^{5+} ions in equilibrium with the much more numerous V^{4+} ions. These V^{5+} ions are possibly associated with V^{4+} in mixed valence pairs. Moreover, the present study has explained why the distinct phases of the reduction by butane and the reoxidation by gaseous oxygen can be performed separately, as is currently done in the new circulating bed process (19–21).

Such a two-step process, typically referred to as a Mars and van Krevelen mechanism, is indeed in agreement with the participation of lattice oxygen as confirmed recently using $^{18}O_2$ (22).

Because of the p-type semiconductive character, we propose that charge carriers are p^+ holes known as strong oxidizing agents. Actually, p^+ holes which are virtual positive charges correspond to O^- species in the solid, which would result from a charge transfer equilibrium creating V^{4+}–O^- ion pairs. Such a reactive pair associating a CUS V^{4+} and O^- species could explain the initial butane activation with hydrogen abstraction by O^- species. The subsequent oxydehydrogenation steps could also occur on V^{4+}–O^- pairs. It is possible that oxygen insertion in the butadiene intermediate could also involve surface lattice O^- species by a mechanism of [4 + 2] cycloaddition.

In addition, electrical conductivity measurements have confirmed that the pyrophosphate phase is the main active phase in activated V–P–O catalysts. In agreement with a previous work using ^{31}P-NMR and XPS (10), V–P–O catalysts activated at 400°C under a butane–air mixture acquire most of their catalytic performance only after at least 84 h.

REFERENCES

1. "Vanadyl Pyrophosphate Catalysts" (G. Centi, Ed.), *Catal. Today* **16** (1993).
2. Hodnett, B. K., *Catal. Rev. Sci. Eng.* **27**, 373 (1986); *Catal. Today* **1**, 477 (1987).
3. Centi, G., Trifirò, F., Ebner, J. R., and Franchetti, J. M., *Chem. Rev.* **88**, 55 (1988).
4. Bordes, E., *Catal. Today* **1**, 499 (1977).
5. Centi, G., *Catal. Today* **16**, 5 (1993).
6. Ben Abdelouahab, F., Olier, R., Guilhaume, N., Lefevre, F., and Volta, J. C., *J. Catal.* **134**, 151 (1992).
7. Volta, J. C., Béré, K., Zhang, Y. J., and Olier, R., *in* "Catalytic Selective Oxidation" (S. T. Oyama and J. W. Hightower, Eds.), ACS Symposium Series, Vol. 523, p. 217. American Chem. Soc., Washington, DC, 1993.
8. Hutchings, G. J., Desmartin-Chomel, A., Olier, R., and Volta, J. C., *Nature* **348**, 41 (1994).
9. Overbeek, R. A., Versluijs-Helder, M., Warringa, P. A., Bosna, E. J., and Geus, J. W., *in* "New Developments in Selective Oxidation Studies in Surface Science and Catalysis" (V. Cortés Corberan and S. Vic Bellon, Eds.), Vol. 82, p. 183, Elsevier, Amsterdam, 1994.
10. Abon, M., Béré, K. E., Tuel, A., and Delichère, P., *J. Catal.* **156**, 28 (1995).
11. Rouvet, F., Herrmann, J.-M., and Volta, J. C., *J. Chem. Soc. Faraday Trans.* **90**, 1441 (1994).
12. Yang, T. C., Rao, K. K., Der Huang, I., and Exxon Res. Eng. Co., U.S. Patent 4,392,986, 1987.
13. Ebner, J. R., and Thompson, M. R., *in* "Structure–Activity and Selectivity Relationship in Heterogeneous Catalysis" (R. K. Grasselli and A. W. Sleight, Eds.), p. 31. Elsevier, Amsterdam, 1991.
14. Herrmann, J.-M., *in* "Catalyst Characterization, Physical Techniques for Solid Materials" (B. Imelik and J. C. Védrine, Eds.), p. 559. Plenum, New York, 1994.
15. van Oeffelen, D. A. G., van Hooff, J. H. C., and Schuit, G. C. A., *J. Catal.* **95**, 84 (1985).
16. Caldararu, M., and lonescu, N. I., *in* "Proceedings, 10th International Congress on Catalysis, Budapest, 1992" (L. Guczi, F. Solymosi, and P. Tétényi, Eds.), p. 1879. Akadémiai Kiadó, Budapest, 1993.
17. Bjorklund, R. B., Odenbrand, C. U. I., Brandin, J. G. M., Andersson, L. A. H., and Liedberg, B., *J. Catal.* **119**, 187 (1989).
18. Herrmann, J.-M., and Pichat, P., *in* "Spillover of Adsorbed Species" (G. M. Pajonk, S. J. Teichner, and J. E. Germain, Eds.), *Stud. Surf. Sci. Catal.*, Vol. 17, p. 77. Elsevier, Amsterdam, 1983.
19. Contractor, R. M., Garnett, D. I., Horowitz, H. Z., Bergan, H. E., Patience, G. S., Schwartz, J. T., and Sisler, G. M., *in* "New Developments in Selective Oxidation II" (V. Cortés Corberan and S. Vic Bellon, Eds.), *Stud. Surf. Sci. Catal.*, Vol. 82, p. 233, Elsevier, Amsterdam, 1994.
20. Contractor, R. M., Bergna, H. E., Horowitz, H. S., Blackstone, C. M., Malone, B., Torardi, C. C., Griffiths, B., Choudhry, U., and Sleight, A. W., *Catal. Today* **1**, 49 (1987).
21. Emig, G., Uihlein, K., and Häcker, C.-J., *in* "New Developments in Selective Oxidation II" (V. Cortès Corberan and S. Vic Bellon, Eds.), *Stud. Surf. Sci. Catal.*, Vol. 82, p. 243, Elsevier, Amsterdam, 1994.
22. Abon, M., Béré, K. E., and Delichère, P., *Catal. Today*, in press.
23. Osburn, C. M., and West, R. W., *J. Chem. Solids* **32**, 1331 (1971).
24. Golunski, S. E, Nevell, T. G., and Hucknall, D. J., *J. Chem. Soc. Faraday Trans. 1* **81**, 1121 (1985).
25. Farrell, F. J., Nevell, T. G., and Hucknall, D. J., *Chem. Soc. Faraday Trans. 1* **82**, 3587 (1986).
26. Herrmann, J.-M., Disdier, J., Gama-Freire, F., and Portela, M. F., *J. Chem. Soc. Faraday Trans.* **91**, 2343 (1995).
27. López-Granados, M., Conesa, J. C., and Fernandez-Garcia, M., *J. Catal.* **141**, 671 (1993).
28. Herrmann, J.-M., Disdier, J., Mozzanega, M. N., and Pichat, P., *J. Catal.* **60**, 369 (1979).
29. Herrmann, J.-M., Courbon, H., Disdier, J., Mozzanega, M.-N., and Pichat, P., *in* "New Developments in Selective Oxidation" (G. Centi and F. Trifirò, Eds.), p. 675. Elsevier, Amsterdam, 1990.

30. Pepera, M. A., Callahan, J. L., Desmond, M. J., Milburger, E. C., Blum, P. R., and Bremer, N. J., *J. Am. Chem. Soc.* **107**, 4883 (1985).
31. Chaar, M. A., Patel, D., Kung, M. C., and Kung, H. H., *J. Catal.* **105**, 483 (1987).
32. Centi, G., Trifirò, F., Busca, G., Ebner, J. R., and Gleaves, J. T., "Proceedings, 9th International Congress on Catalysis, Calgary, 1988" (M. J. Phillips and M. Ternan, Eds.), Vol. 4, p. 1538. Chem. Institute of Canada, Ottawa, 1988.
33. Centi, G., Fornasari, G., and Trifirò, F., *J. Catal.* **89**, 44 (1984).
34. Matsuura, I., *in* "Proceedings, 8th International Congress on Catalysis, Berlin, 1984," Vol. IV, p. 473. Dechema, Frankfurt-am-Main, 1984.
35. Szakacs, S., Wolf, H., Mink, G., Bertoli, I., Wüstneck, N., Lücke, B., and Seeboth, H., *Catal. Today* **1**, 27 (1987).
36. Aika, K., and Lunsford, J. H., *J. Phys. Chem.* **81**, 1393 (1977).
37. Béré, K. E., Gravelle, M., and Abon, M., *J. Chim. Phys.* **92**, 1521 (1995).
38. Cavani, F., Centi, G., and Trifirò, F., *J. Chem. Soc. Chem. Commun.* 492 (1985).
39. Busca, G., Centi, G., and Trifirò, F., *Appl. Catal.* **25**, 265 (1986).
40. Cornaglia, L. M., Lombardo, E. A., Anderson, J. A., and Fierro, J. L. G., *Appl. Catal. A* **100**, 37 (1993).
41. Busca, G., *Catal. Today* **27**, 457 (1996).
42. Gai, P. L., and Kourtakis, K., *Science* **267**, 661 (1995).
43. Busca, G., Ramis, G., and Lorenzelli, V., *J. Mol. Catal.* **50**, 231 (1989).
44. Busca, G., Centi, G., Trifirò, F., and Lorenzelli, V., *J. Phys. Chem.* **90**, 1337 (1986).
45. Béré, K. E., Ph.D. Thesis, Université de Lyon, No. 38-96, 1996.